

## HiSST: 4th International Conference on High-Speed Vehicle Science Technology 22 -26 September 2025, Tours, France



# Experimental Investigation of a Disk-Shaped RDRE Operating with Liquid Propane and Liquid Nitrous Oxide

Gyeong-Ui Mo<sup>1</sup>, Keon-Hyeong Lee<sup>1</sup>, Su-Wan Choi<sup>1</sup>, Min-Seon Jo<sup>1</sup> and Jeong-Yeol Choi<sup>2</sup>

#### **Abstract**

This study experimentally investigates the operating characteristics of a disk-shaped rotating detonation rocket engine (Disk-RDRE) fueled with liquid nitrous oxide (N<sub>2</sub>O) and propane (C<sub>3</sub>H<sub>8</sub>), exploiting their inherent self-pressurizing properties. Two operating conditions were examined by varying the total mass flow rate while maintaining a fixed equivalence ratio of 1.18. Combustion dynamics were captured using high-speed imaging in conjunction with FFT and STFT analyses to assess detonation wave propagation and frequency characteristics. In both cases, the engine sustained a stable single-wave detonation mode, with operating frequencies on the order of 6–7 kHz and propagation velocities reaching approximately 80% of the theoretical Chapman–Jouguet (C–J) velocity. Visualization further confirmed that the detonation front preserved a consistent rotational direction and propagated tangentially along the combustor wall. These results experimentally validate the feasibility of stable liquid-propellant operation in a disk-shaped RDE and provide a foundation for the future development of liquid-based detonation propulsion systems.

Keywords: Liquid propellant, self-pressurized propellant, Disk-RDRE, Detonation Wave propagation

## 1. Introduction

Detonation-based propulsion has long been recognized as a promising approach to overcoming the thermodynamic limitations of conventional constant-pressure combustion systems. In recent years, significant research efforts have also been undertaken at national laboratories such as NASA, with rotating detonation engines (RDEs) attracting increasing attention as next-generation propulsion systems due to their potential for both structural simplification—such as reduced combustor size—and performance enhancement [1-2]. Kailasanath [3-4] provided comprehensive reviews of detonation-based propulsion, highlighting the theoretical advantages of detonation cycles as well as the progress and challenges identified in early pulse detonation engine (PDE) studies. Building on this foundation, Kim et al. [5-6] reviewed fundamental and application-oriented advances in RDE research, positioning the RDE as a leading candidate for future aerospace propulsion.

Extensive numerical investigations have elucidated key mechanisms governing detonation propagation and stability. Choi et al. [7] established resolution and domain-length requirements necessary to capture detonation cellular structures in simulations. Lee et al. [8] analyzed curvature effects in annular channels and identified a critical radius ratio for stable propagation. Niyasdeen et al. [9] introduced a chemical-timescale framework to interpret stability across equivalence ratios, while Pavalavanni et al. [10] applied modal decomposition to characterize bifurcation phenomena in cellular detonations. Extending the analysis of geometric effects, Niyasdeen et al. [11] demonstrated through numerical studies that annular dimensionless radius strongly governs propagation in both circular and noncircular RDEs.

HiSST-2025-145 Page | 1

<sup>&</sup>lt;sup>1</sup> Graduate Research Assistant, Pusan National University, Busan 46241, Republic of Korea

<sup>&</sup>lt;sup>2</sup> Professor, Pusan National University, Busan 46241, Republic of Korea, <u>aerochoi@pusan.ac.kr</u> (Corresponding)

Experimental investigations have further validated the operability of RDEs across diverse conditions. Han et al. [12] reported fundamental operating characteristics using gaseous propellants. Koo et al. [13] showed that rectangular-hole injectors enhance detonation stability compared with slit-type designs. Lee et al. [14] experimentally confirmed the feasibility of noncircular (tri-arc) combustors, while Mo et al. [15] demonstrated that fuel-jet penetration—achieved through jet-in-supersonic-crossflow injection—critically governs mode transitions between stable detonation, chaotic propagation, and deflagration-like behavior.

More recently, increasing attention has been directed toward liquid-propellant rotating detonation engines (RDEs), advancing their potential for practical rocket propulsion applications. Sato et al. [16] systematically characterized the combustion structure of an liquid ethanol/N<sub>2</sub>O cylindrical RDE, elucidating the influence of oxidizer vapor quality, injector stiffness, and fuel temperature on detonation stability and wall erosion. Teasley et al. [17] demonstrated long-duration operation of additively manufactured LOX/H<sub>2</sub> and LOX/CH<sub>4</sub> RDEs, achieving cumulative run times of up to 802 s with thrust levels exceeding 4000 lbf.

Flight demonstrations have further validated detonation operation under relevant environments. Kawalec et al. [18] reported successful ground and short-duration flight operation of a regeneratively cooled conical RDE fueled with  $N_2O/C_3H_8$ , reaching an altitude of 450 m. Goto et al. [19] achieved the first in-space demonstration of an RDE on JAXA's S-520-31 rocket, sustaining gaseous CH<sub>4</sub>/O<sub>2</sub> detonation for  $\sim$ 6 s above 100 km altitude. More recently, Sato et al. [20] demonstrated a bipropellant ethanol/N<sub>2</sub>O RDE on the S-520-34 under vacuum conditions.

Collectively, these numerical investigations, laboratory experiments, and flight demonstrations have markedly advanced the technical maturity of detonation-based propulsion. Nevertheless, most prior work has been constrained to gaseous propellants or conventional annular and cylindrical geometries. To address this gap, the present study introduces the design and experimental evaluation of a disk-shaped rotating detonation rocket engine (Disk-RDRE) intended for the second stage of a small sounding rocket. liquid nitrous oxide and propane are employed as propellants, exploiting their self-pressurizing capability at ambient temperature. The disk-shaped configuration, characterized by a reduced chamber height relative to annular designs, offers advantages in volume and weight reduction. Building on prior demonstrations with a gaseous ethylene—oxygen Disk-RDRE, the present work extends the concept to a fully liquid-propellant system. The objectives are twofold: (i) to demonstrate stable detonation operation with liquid propellants in a disk geometry and (ii) to quantitatively characterize operating performance, thereby providing new experimental evidence for the applicability of liquid-based Disk-RDREs in advanced rocket propulsion.

## 2. Experimental Setup

## 2.1. Disk-RDRE Configuration

The engine investigated in this study employed liquid nitrous oxide and propane as propellants. The combustor was specifically designed for ground testing of a liquid-propellant rotating detonation rocket engine (RDRE) to assess its performance and operating characteristics. To facilitate quantitative diagnostics, the central section of the combustor was modularized, allowing the installation of interchangeable pure-quartz windows and dynamic pressure sensors.

The combustor had an inner diameter of 100 mm and a channel height of 5.5 mm, and the main body was fabricated from SUS316 stainless steel. Pressure sensor ports were machined from the same material to ensure structural integrity and consistency. Given that the total combustion duration was less than 1 s, and a simplified combustor configuration was adopted.

Figure 1(a) presents a cross-sectional view of the Disk-RDRE. A hole-type injector was implemented, with orifice diameters determined by back-calculating the design flow rate ( $\dot{m}=373$  g/s) using the orifice flow equation. The oxidizer and fuel injector diameters were 0.63 mm and 0.25 mm, respectively. A total of 60 injector holes were manufactured by electrical discharge machining and arranged in an unlike-doublet pattern to promote effective propellant mixing. The injector array was positioned at a radius of 49 mm from the chamber centerline, evenly distributed around the circumference, and oriented at a 45° injection angle. Under the assumption of linear jet trajectories, the oxidizer and fuel streams were designed to impinge at a radial distance of 46.25 mm from the chamber center.

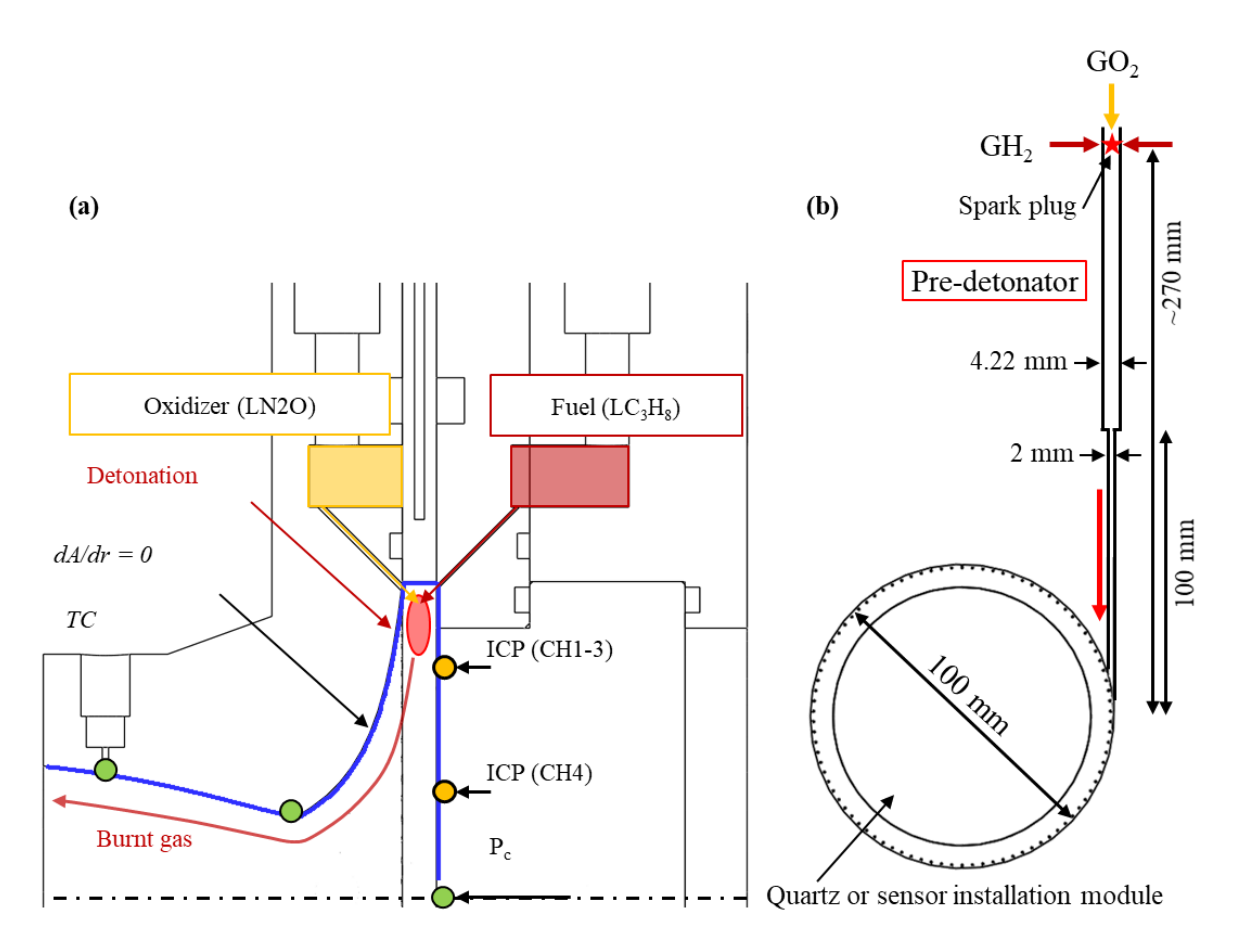


Fig 1. Schematic of cross-section of (a) the Disk-RDRE, (b) Pre-detonator(PDT)

Figure 1(b) depicts the pre-detonator (PDT) employed to initiate ignition of the Disk-RDRE. The PDT operated with gaseous hydrogen and oxygen propellants, a combination extensively validated in prior studies for reliable detonation initiation. The PDT tube was designed with an inner diameter of 4.22 mm, while the connecting tube—responsible for delivering high-enthalpy ignition products into the combustor—was fabricated with a reduced diameter of 2.00 mm. This reduction was necessitated by the low channel height of 5.5 mm, which imposed machining constraints.

The overall length of the PDT was approximately 270 mm, and ignition was achieved using a spark plug energized by a spark coil. The ignition location was aligned with the oxidizer–fuel jet impingement point inside the combustor, while the PDT itself was mounted tangentially along the outer wall of the chamber to ensure effective coupling with the detonation process.

### 2.2. Design of Orifice

The liquid nitrous oxide and propane employed in this study possess self-pressurizing characteristics, enabling propellant delivery to the combustor without the need for an external pressurization system. In conventional gaseous propellant supply systems, mass flow regulation is typically achieved using pressure regulators or mass flow controllers (MFCs). However, when applied to liquid nitrous oxide, the pressure drop across a regulator can induce undesirable phase transitions. To mitigate this effect, an orifice was fabricated, as shown in Figure 4, and subsequently installed upstream of the combustor, as illustrated in Figure 2, thereby minimizing phase change arising from pressure losses.

All experiments were conducted under liquid-phase propellant conditions. The experimental sequence began with relatively low mass flow rates and was progressively extended to higher values, thereby enabling the characterization of a broader operating envelope. The total propellant mass discharged during each run was measured using a load cell and converted into a time-averaged mass flow rate by normalization with respect to the elapsed time, as expressed in Eq. (1). The measured flow rates were then compared with theoretical predictions obtained from the ideal orifice equation, as given in Eq. (2). From this comparison, a discharge coefficient  $C_{\rm d}$  was determined, quantifying deviations from idealized flow behavior caused by viscous losses and flow contraction. Finally, the experimentally obtained  $C_{\rm d}$ 

HiSST-2025-145 Page | 3 Experimental Investigation of a Disk-Shaped RDRE Operating with Liquid Propane and Liquid Nitrous Oxide

was applied as a correction factor to the orifice-based mass flow evaluation using Eq. (3), thereby improving the accuracy of subsequent flow rate estimates.

$$\dot{m}_{actual} = \frac{\Delta m}{t} \tag{1}$$

$$\dot{m}_{ori,ideal} = A\sqrt{2\rho_1 \Delta P} \tag{2}$$

$$\dot{m}_{ori,actual} = \frac{C_d A_{ori}}{\sqrt{1-\beta^4}} = \sqrt{2\rho_1 \Delta P}$$
 (3)

where  $\dot{m}$  is the mass flow rate [kg/s],  $C_d$  is the coefficient of discharge, A is the orifice area [m<sup>2</sup>],  $\rho_1$  is the fluid density [kg/m<sup>3</sup>], and  $\Delta P$  is the pressure drop across the orifice [Pa].

$$\beta = d/D \tag{4}$$

In addition,  $\beta$  denotes the diameter ratio of the orifice diameter d to the pipe diameter D which is dimensionless.

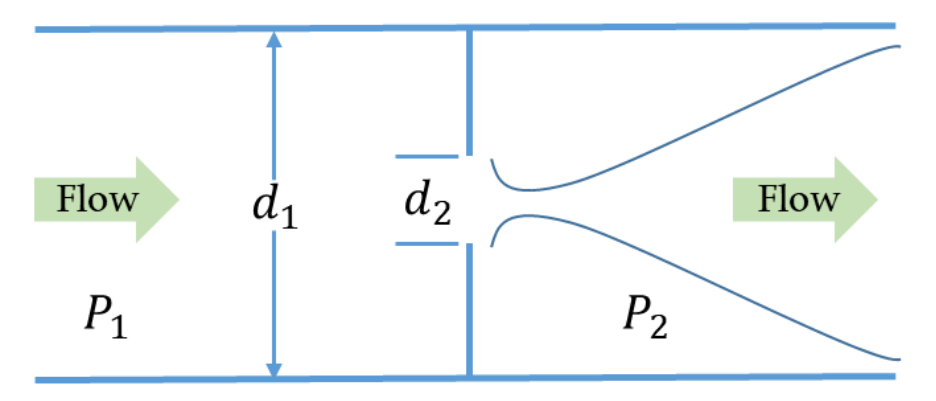


Fig 2. Geometry of the Orifice

The operating altitude of the upper-stage engine was set to 1.4–2.58 km [22], where the ambient pressure decreases from 0.85 to 0.74 bar according to the standard atmosphere. Using RPA software, a bell nozzle was designed for a chamber pressure of 10 bar to deliver more than 600 N of thrust. The TIC (Truncated Ideal Contoured) method was applied to shorten the nozzle length, with an efficiency range of 80–100% considered in the analysis. The results indicated that maximum performance is achieved at an O/F ratio of 8.409 (equivalence ratio of 1.187). As shown in Figure 3, the engine produces more than 600 N of thrust from 1.4 km altitude and maintains a specific impulse above 160 s across the entire operating altitude range.

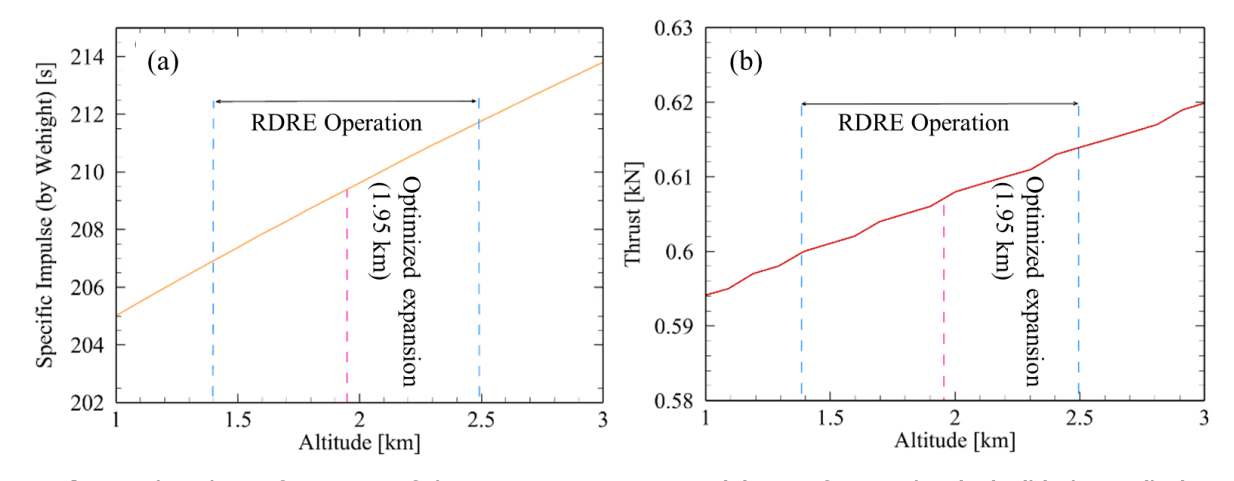


Fig 3. Altitude performance of the upper-stage engine: (a) specific impulse ( $I_{sp}$ ), (b) thrust (kN)

The propellant mass flow rates were determined with consideration of the equivalence ratio. In this study, however, the equivalence ratio was fixed at 1.18 to maintain consistent mixture conditions, while only the total mass flow rate was varied to evaluate the operating characteristics of the combustor. The corresponding orifice diameters employed for each test condition are summarized in Table 1.

Case	Propellant	m (g/s)	Diameter (mm)
Case 1	Nitrous Oxide	89.4	1.77
Case 1	Propane	10.6	0.7
Case 2	Nitrous Oxide	178.7	2.51
Case 2	Propane	21.3	0.99

**Table 1.** Designed Orifice Diameter

## 2.3. Configuration of the Supply System

A schematic of the propellant supply system employed in this study is presented in Figure 4. For the experiments, liquid nitrous oxide cylinders (47 L, 25 kg) and liquid propane cylinders (10 L and 47 L, 10 kg) were used to provide low- and high-flow conditions, respectively. Propellant delivery to the Disk-RDRE was regulated by pneumatic valves (TS06 series, Tootech, Yongin, Republic of Korea).

The PDT was supplied through an auxiliary feed line with gaseous hydrogen (40 L) and gaseous oxygen (40 L) as propellants. The PDT supply pressure was controlled using a spring-loaded regulator (RSN2 series, Swagelok Inc., Solon, USA). After each test, nitrogen gas (40 L) was introduced to purge the combustor and feed lines. The nitrogen purge system was actuated via solenoid valves (121KBG2 series, Parker, Cleveland, USA) connected to both the fuel and oxidizer supply lines.

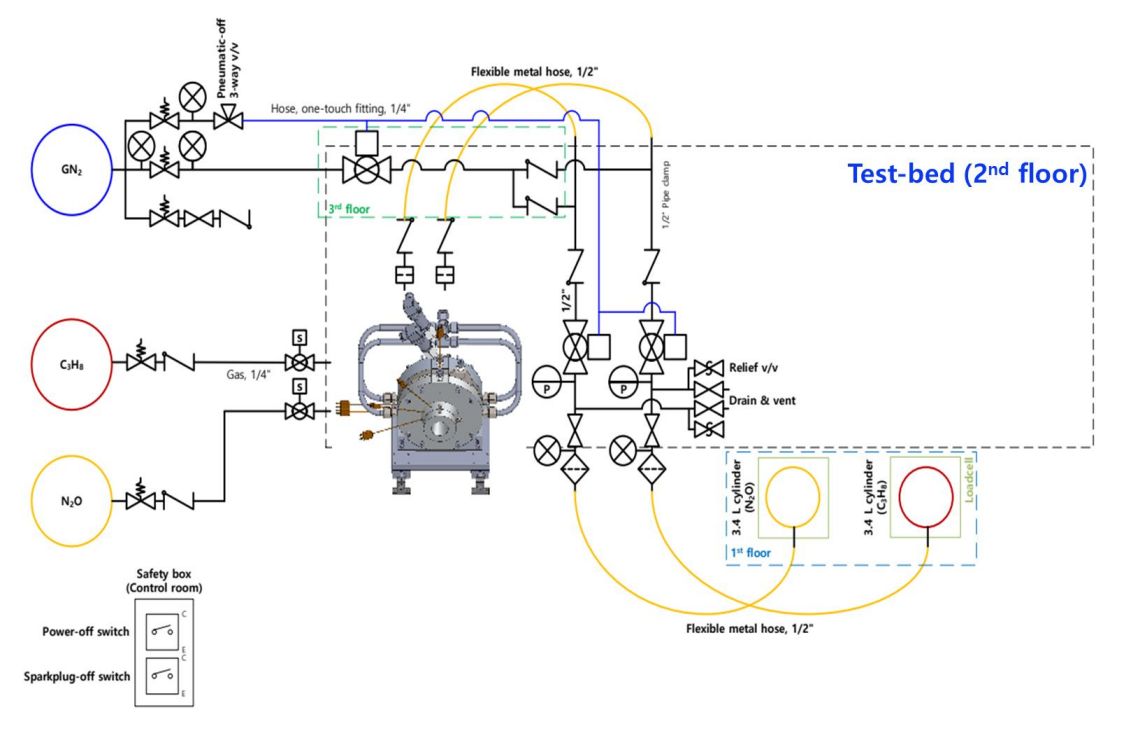


Fig 4. Schematic of Propellant Supply System

## 2.4. Data Acquisition and Control System

A range of instrumentation and control devices was employed to measure key physical quantities during the experiments. Pressures at multiple locations—including the combustor chamber, propellant feed lines, upstream and downstream of the orifice, and the plenum—were measured using S-20 series sensors (WIKA, Klingenberg am Main, Germany), with analog signals acquired via an NI 9205 module. Thrust was measured using an SBA-series load cell (CAS, Yangju, Republic of Korea), with signal amplification provided by a WTM-500 amplifier (CAS). Temperature measurements were obtained using K-type thermocouples (Omega, Norwalk, CT, USA)

Dynamic pressure data were acquired using 113B24 sensors (PCB, Depew, NY, USA), with signals conditioned by a 482C05 signal conditioner (PCB). Three sensors were mounted circumferentially at a radius of 36.5 mm with 45° spacing, and an additional sensor was positioned at a radius of 23 mm. All

HiSST-2025-145 Page | 5 Experimental Investigation of a Disk-Shaped RDRE Operating with Liquid Propane and Liquid Nitrous Oxide

signals were recorded with a DL850E Scopecorder (Yokogawa, Tokyo, Japan). To reduce the risk of sensor damage during detonation, the sensors were installed in a recessed configuration. The acquired data were subsequently analyzed using FFT and STFT techniques to characterize operating frequencies.

To capture detonation phenomena inside the combustor, the Disk-RDRE was designed with an interchangeable central module, enabling the installation of either dynamic pressure sensor ports or a quartz observation window. Figure 5(a) presents the optical field available with the quartz window installed, while Figure 5(b) illustrates the configuration of the dynamic pressure sensors. Owing to injector interference, the quartz window inner diameter was limited to 85 mm.

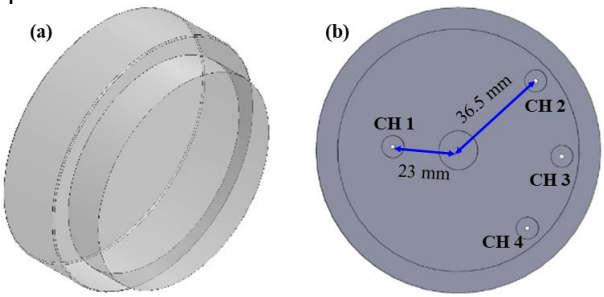


Fig 5. 3D model of the combustor with (a) quartz window and (b) dynamic pressure sensor ports

In addition, a Phantom v2512 high-speed camera (Phantom, Wayne, NJ, USA) was employed to visualize combustion phenomena inside the chamber through the quartz window. During operation, a planar optical mirror was positioned to redirect the optical path by 90°, enabling direct observation of the Disk-RDRE combustor. The operating parameters of the high-speed camera are summarized in Table 2.

Resolution	Sample rate	Period	Exposure	EDR	Case
256 x 256	200,000 fps	<b>5.00</b> μs	<b>0.40</b> μs	<b>0.00</b> μs	Case 1
256 x 256	200,000 fps	<b>5.00</b> μs	<b>0.40</b> μs	<b>0.00</b> μs	Case 2

**Table 2.** High-speed camera recording condition

Figure 6 presents a schematic arrangement of the high-speed and digital cameras. Owing to the use of a planar optical mirror, the images captured by the high-speed camera were laterally inverted relative to the actual configuration. Figure 6 highlights the distinction between the recorded images and the true physical orientation. Importantly, the rotation direction of the detonation wave observed in the high-speed recordings appeared reversed with respect to the actual propagation direction; this inversion was therefore carefully accounted for during data analysis.

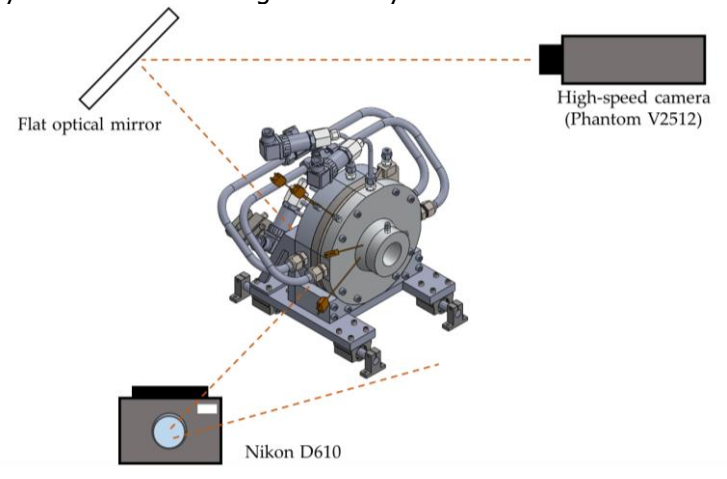


Fig 6. Schematic arrangement of the high-speed and digital cameras

## 2.5. Analysis Methods for High-Speed Imaging

To analyze detonation wave propagation inside the chamber, high-speed camera images were

processed to extract luminosity, perform FFT and STFT analyses, and generate unwrapped images. The unwrapping procedure followed a method similar to that proposed by Bennewitz et al. [21]. For each case, 1,000–3,000 frames were used in the analysis, with 1,000 frames corresponding to approximately 5 ms of physical time.

During preprocessing, a composite image was generated by summing the maximum luminosity at each pixel across all frames, while pixel intensities below a prescribed threshold were set to zero. To exclude the edge region of the quartz observation window, Canny edge detection was applied, followed by circle detection using the Hough transform. Unwrapped images were then constructed by sampling at 90% of the detected circle radius and mapping the pixel intensities from 0° to 360° along the horizontal axis. Finally, luminosity data extracted at the 0° position were used to perform FFT and STFT analyses for frequency characterization.

#### 3. Results and Discussion

#### 3.1. Experimental Sequence

Figure 7 illustrates the sequence of the experimental procedure. First, the pneumatic valve supplying propellants to the Disk-RDRE and the solenoid valves for the PDT fuel and oxidizer were opened. Due to pipeline length and signal transmission delay, the pressure upstream of the orifice increased approximately 0.4 s after the input signal triggered the valve opening.

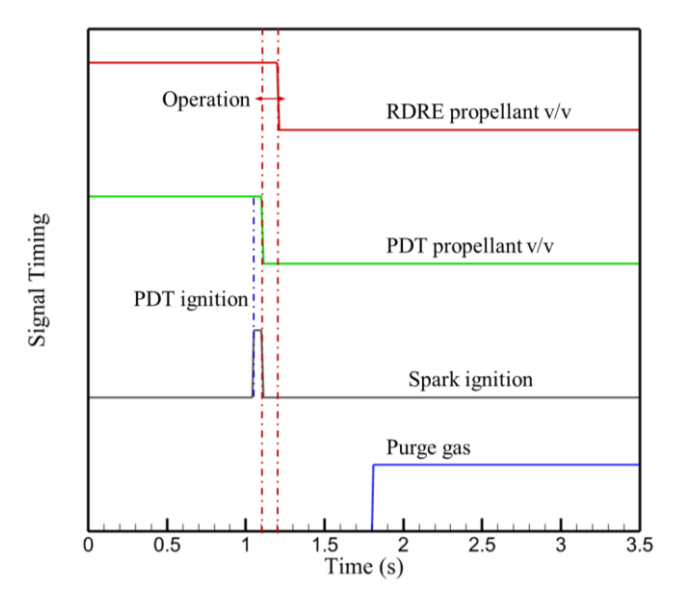


**Fig 7.** Sequence of the experimental procedure

#### 3.2. Result

The experiments were conducted under two total mass flow rate conditions, 50 g/s and 100 g/s. Following PDT ignition, the ignition process of the Disk-RDRE combustor and the subsequent stabilization of the detonation wave were examined, corresponding to Case 1 (50 g/s) and Case 2 (100 g/s), respectively. In both cases, high-speed imaging was employed to confirm detonation wave propagation, construct unwrapped images, and perform FFT and STFT analyses based on luminosity data. In Case 1, no pressurization was applied to the propane tank, whereas in Case 2 helium pressurization at 13.79 bar (200 psi) was introduced.

Figure 8 presents the detonation wave propagation observed in Case 1 at an equivalence ratio of 1.18. Under this condition, the detonation propagated in a stable single-wave (1-wave) mode, although the rotation direction was reversed relative to Case 2. The operating frequency in Case 1 ranged from 6.8 to 13.5 kHz. FFT analysis provided the average operating frequency of the Disk-RDRE but could not resolve temporal variations, whereas STFT analysis enabled the identification of frequency changes over time at the expense of spectral resolution. By comparing FFT and STFT results, the specific time intervals at which dominant frequencies shifted could be clearly identified.

HiSST-2025-145 Page | 7 Experimental Investigation of a Disk-Shaped RDRE Operating with Liquid Propane and Liquid Nitrous Oxide

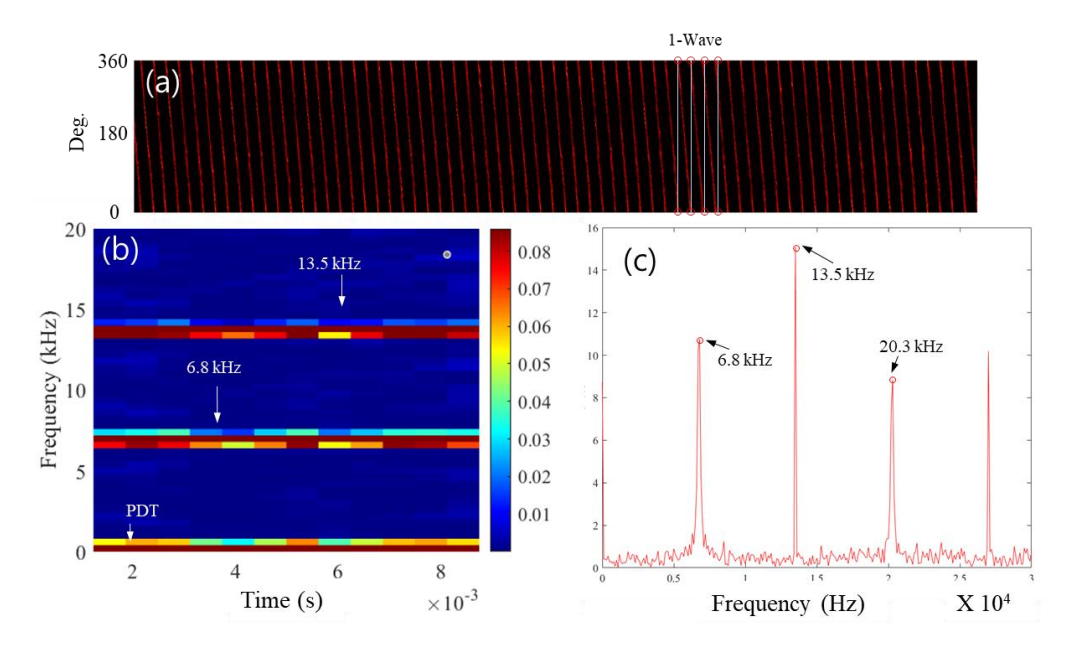
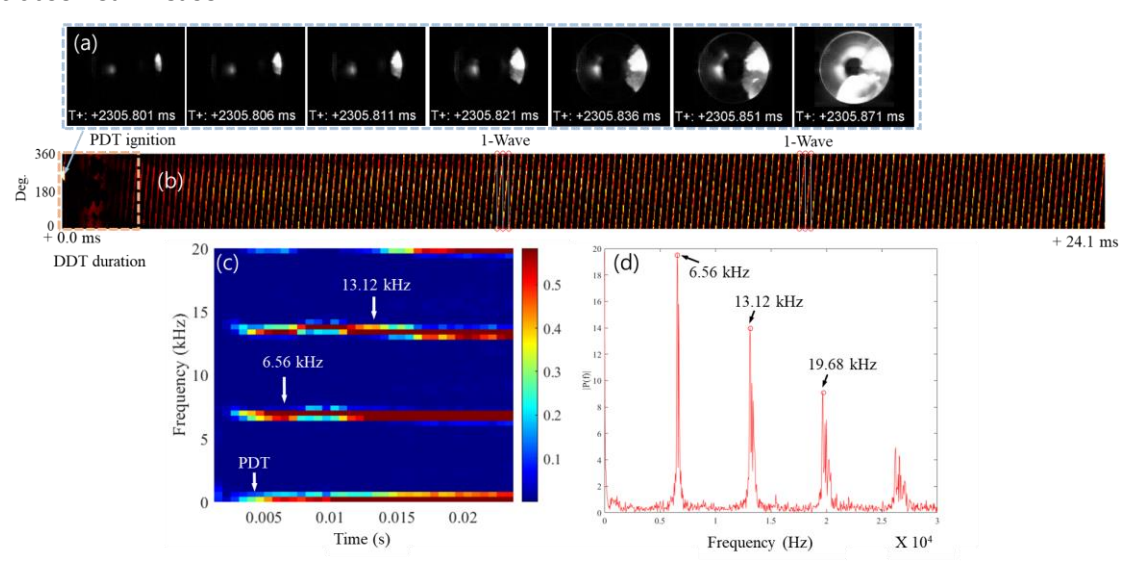


Fig 8. Post-processed results for Case 1: (a) unwrapped RDE image, (b) STFT analysis, and (c) FFT analysis

Figure 9 illustrates the sequence of detonation development and stabilization following PDT ignition under Case 2 conditions. During the initial 0.07 ms, a strong detonation wave generated by the PDT propagated into the combustor, after which a deflagration-to-detonation transition (DDT) occurred, leading to the full development of the detonation wave. The wave subsequently stabilized, propagating in a single-wave (1-wave) mode, consistent with Case 1. Despite the higher total mass flow rate and the application of pressurization in Case 2, the detected operating frequency remained comparable to that observed in Case 1.



**Fig 9.** Post-processed results for Case 2: (a) detonation development after PDT ignition, (b) unwrapped RDE image, (c) STFT analysis, and (d) FFT analysis

FFT and STFT analyses confirmed that comparable operating frequencies were obtained under both conditions. Based on these results, the detonation velocity was calculated from the peak frequency identified in the STFT analysis using the following relation (5):

$$V_{exp} = 2\pi r f_{peak}/N \tag{5}$$

Here,  $V_{exp}$  denotes the experimentally obtained detonation velocity [m/s],  $f_{peak}$  is the detected detonation frequency [kHz], r represents the combustor radius [m], N is the number of detonation waves.

The experimentally obtained velocities were then compared with the theoretical Chapman–Jouguet (C–J) velocity. The C–J velocity was calculated using NASA-CEA at a stoichiometric mixture ratio of 9.97 and an initial temperature of 293 K. As summarized in Table 3, the experimental detonation velocities corresponded to approximately 79–82% of the theoretical C–J value.

<b>Table 3.</b> Summary of exper	mental conditions and results
----------------------------------	-------------------------------

Case	Wave No.	$f_{peak}$	$V_{exp}$	C-J Velocity Deficit
1	1-wave	6.8 kHz	1976 m/s	82 %
2	1-wave	6.56 kHz	1906 m/s	79.7 %

Figure 10 presents a time-sequenced set of high-speed camera images capturing flame evolution inside the combustor for Case 2. The sequence clearly visualizes the detonation wave propagation process, in which a single flame front is consistently observed at all time steps, confirming stable operation in a 1-wave mode. The flame front also maintained a uniform rotational direction and exhibited a pronounced tendency to propagate tangentially along the combustor wall. These results demonstrate not only the stable propagation of the detonation wave but also the role of combustor wall interactions in directing the flow field.

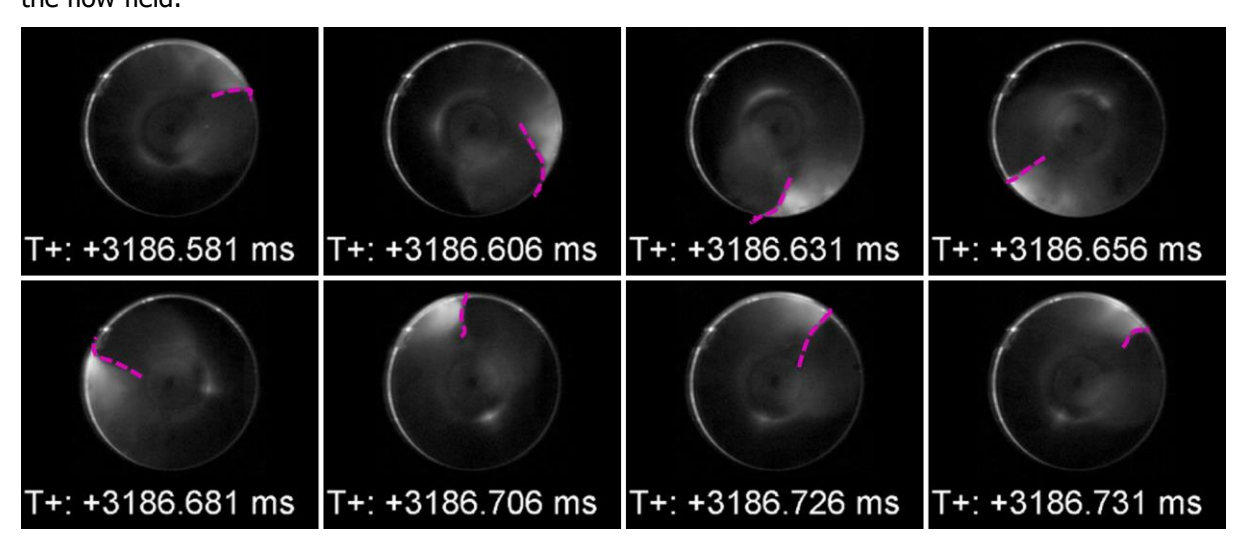


Fig 10. High-speed images of Case 2 showing detonation propagation

#### 4. Conclusion

This study experimentally investigated the stable operating conditions of a disk-shaped rotating detonation rocket engine (Disk-RDRE) fueled with self-pressurizing liquid nitrous oxide and propane. Experiments were conducted at total mass flow rates of 50 g/s (case 1) and 100 g/s (case 2) with the equivalence ratio fixed at 1.18. In both cases, detonation propagated in a stable 1-wave mode. FFT analysis revealed operating frequencies of 6.8 kHz and 6.56 kHz, indicating consistent behavior irrespective of mass flow rate. The detonation propagation velocity estimated from the peak frequency corresponded to approximately 79.7–82% of the theoretical Chapman–Jouguet (C–J) velocity, demonstrating close agreement with theoretical predictions.

High-speed imaging further visualized the propagation sequence of the detonation wave inside the combustor. A single flame front was observed throughout all time steps, confirming stable single-wave operation. The flame front maintained a uniform rotational direction and exhibited a pronounced tendency to propagate tangentially along the combustor wall.

These results experimentally confirm the feasibility of stable operation in a liquid-propellant Disk-RDRE and provide fundamental data to support design considerations for future liquid-based detonation propulsion systems. Nevertheless, as this work represents a preliminary experimental study, quantitative evaluation of performance metrics such as thrust, combustion efficiency, and long-duration stability remains limited. Future research should therefore include comprehensive performance assessments to address these aspects.

HiSST-2025-145 Page | 9 Experimental Investigation of a Disk-Shaped RDRE Operating with Liquid Propane and Liquid Nitrous Oxide Copyright © 2025 by author(s)

#### References

- 1. Teasley, T. ECI Final Report: Closing of Critical Technology Gaps for Rotating Detonation Rocket Engines. (2024)
- 2. Teasley, T. NASA's Rotating Detonation Rocket Engine Development. In *47th Annual AAS Guidance, Navigation and Control (GN&C) Conference.* (2025)
- 3. Kailasanath, K. Review of propulsion applications of detonation waves. *AIAA journal.* 38.9, 1698-1708 (2000)
- 4. Kailasanath, Kailas. Recent developments in the research on pulse detonation engines. *AIAA journal.* 41.2, 145-159 (2003)
- 5. Kim, J. M., Niyasdeen, M., Han, H. S., Oh, S., & Choi, J. Y. Research activities on PGC propulsion based on RDE, part I: basic studies. *Journal of the Korean Society of Propulsion Engineers*. 21(5), 97-107 (2017)
- Kim, J. M., Niyasdeen, M., Han, H. S., Oh, S., & Choi, J. Y. Research Activities on PGC Propulsion Based on RDE, Part II: Application Studies. *Journal of the Korean Society of Propulsion Engineers*. 21(6), 91-102 (2017)
- 7. Choi, J. Y., Ma, F., & Yang, V. Numerical Simulation of Cellular Structure of Two-Dimensional Detonation Waves. In *43rd AlAA Aerospace Sciences Meeting and Exhibit*. 1174 (2005)
- 8. Lee, S., Cho, D. R., & Choi, J. Y. Effect of curvature on the detonation wave propagation characteristics in annular channels. In *46th AIAA Aerospace Sciences Meeting and Exhibit*,. 988 (2008)
- 9. Nejaamtheen, M. N., Sung, B. K., & Choi, J. Y. Numerical Analysis of the Characteristic Chemical Timescale of a C2H4/O2 Non-Premixed Rotating Detonation Engine. *Energies*. *18*(4), 989 (2025)
- 10. Pavalavanni, P. K., Kim, J. E., Jo, M. S., & Choi, J. Y. Numerical investigation of the detonation cell bifurcation with decomposition technique. *Aerospace*, *10*(3), 318 (2023)
- 11. Nejaamtheen, M. N., Kim, T. Y., Pavalavanni, P. K., Ryu, J., & Choi, J. Y. Effects of the dimensionless radius of an annulus on the detonation propagation characteristics in circular and non-circular rotating detonation engines. *Shock Waves*, *31*(7), 703-715 (2021)
- 12. Han, H. S., Lee, E. S., & Choi, J. Y. Experimental investigation of detonation propagation modes and thrust performance in a small rotating detonation engine using C2H4/O2 propellant. *Energies*, 14(5), 1381 (2021)
- 13. Koo, I. H., Lee, K. H., Kim, M. S., Han, H. S., Kim, H., & Choi, J. Y. Effects of injector configuration on the detonation characteristics and propulsion performance of rotating detonation engine (RDE). *Aerospace*, *10*(11), 949 (2023)
- Lee, J. H., Ryu, J. H., Lee, E. S., Han, H. S., & Choi, J. Y. Experimental proof of concept of a noncircular rotating detonation engine (RDE) for propulsion applications. *Aerospace*, 10(1), 27 (2023)
- 15. Mo, G. U., Koo, I. H., Lee, K. H., Choi, S. W., & Choi, J. Y. Effects of Fuel Penetration on the RDE Performance with JISC Injector Configuration. *Aerospace*, *11*(9), 752 (2024)
- 16. Sato, T., Nakata, K., Ishihara, K., Itouyama, N., Matsuoka, K., Kasahara, J., ... & Funaki, I. Combustion structure of a cylindrical rotating detonation engine with liquid ethanol and nitrous oxide. *Combustion and Flame*, 264, 113443 (2024)
- Teasley, T. W., Fedotowsky, T. M., Gradl, P. R., Austin, B. L., & Heister, S. D. Current state of NASA continuously rotating detonation cycle engine development. In *AIAA SciTech 2023 Forum.* 1873 (2023).
- 18. Kawalec, M., Wolański, P., Perkowski, W., & Bilar, A. Development of a liquid-propellant rocket powered by a rotating detonation engine. *Journal of Propulsion and Power*, 39(4), 554-561 (2023)

- 19. Goto, K., Matsuoka, K., Matsuyama, K., Kawasaki, A., Watanabe, H., Itouyama, N., ... & Yamada, K. Flight demonstration of detonation engine system using sounding rocket S-520-31: performance of rotating detonation engine. In *AIAA Scitech 2022 Forum*. 0232 (2022)
- 20. Sato, T., Matsuoka, K., Itouyama, N., Yasui, M., Matsuyama, K., Ide, Y., ... & Yahata, Y. Flight Demonstration of Detonation Engine System Using Sounding Rocket S-520-34: Performance of Rotating Detonation Engine Using Liquid Propellants. In *AIAA SCITECH 2025 Forum.* 0174 (2025).
- 21. Bennewitz, J. W., Bigler, B. R., Hargus, W. A., Danczyk, S. A., & Smith, R. D. Characterization of detonation wave propagation in a rotating detonation rocket engine using direct high-speed imaging. In *2018 Joint Propulsion Conference*. 4688 (2018)
- 22. Oh, J. Sounding Rocket System Design and Technical Management Process Optimization Study Using MBSE (Master's thesis). Department of Aerospace Engineering, Pusan National University. (2023)

HiSST-2025-145